Chinese Chemical Letters 36 (2025) 110528

Contents lists available at ScienceDirect

Chinese Chemical Letters

journal homepage: www.elsevier.com/locate/cclet

Evaluating the global thiols redox state in living cells using a reducing sulfur species responsive fluorescence switching platform

Hui Zhang[a], Rong Feng[a], Wanyi Yu[a], Hongbei Wei[a], Tianhong Wu[a], Peng Zhang[a], Wenhai Bian[a], Xin Li[a], Di Gao[a], Guojun Weng[a], Zhe Yang[a], Tony D. James[b,c], Xiaolong Sun[a,*]

[a] The Key Laboratory of Biomedical Information Engineering of Ministry of Education, School of Life Science and Technology, Xi'an Jiaotong University, Xi'an 710049, China
[b] Department of Chemistry, University of Bath, Bath BA2 7AY, United States
[c] School of Chemistry and Chemical Engineering, Henan Normal University, Xinxiang 453007, China

ARTICLE INFO

Article history:
Received 17 July 2024
Revised 30 September 2024
Accepted 7 October 2024
Available online 10 October 2024

Keywords:
Fluorescent probe
Reducing sulfur species
Donor-excited photo-induced electron transfer
Thiols redox state
Ferroptosis

ABSTRACT

Redox dyshomeostasis is a critical factor in the initiation of numerous diseases, making the accurate evaluation of the redox status of the cellular environment an important aspect of physiological research. However, maintaining redox homeostasis relies on a complex and dynamic physiological system involving multiple substrate-enzyme interactions, so its accurately detection remains a challenge. With this research, we developed an activable fluorescence switching platform by incorporating different conjugate acceptors to a fluorophore using ester bonds and resulting in fluorescence quenching due to donor-excited photo-induced electron transfer (*d*-PeT), which was confirmed through density functional theory calculations. The reaction-based probe was deployed for recognizing all major intracellular reducing sulfur species (RSS), including H_2S, cysteine (Cys), homocysteine (Hcy), glutathione (GSH), and protein free thiols. The quenched fluorescence was significantly recovered by RSS, through releasing the fluorophore and diminishing the *d*-PeT effect. Furthermore, the fluorescent probe was used for the sensing and imaging RSS in living cells, demonstrating good cell-permeability, low cytotoxicity, and negative correlation with reactive oxygen species content, enabling the evaluating of global thiols redox state in HepG2 cellular lines during ferroptosis processes.

Intracellular redox homeostasis is essential for maintaining normal cell growth and metabolic state [1,2]. Excessive levels of oxidants are associated with ageing and numerous diseases [3,4]. To sustain the oxidation–reduction balance, a complex intracellular antioxidant system and regulatory network is in place. This system involves a variety of substances with short lifetimes and high activities, such as reactive oxygen species (ROS, *e.g.*, superoxide anion and H_2O_2) [5], reactive sulfur species (*e.g.*, hydrogen sulphide (H_2S)) [6,7], biothiols (cysteine (Cys), glutathione (GSH)) [8], nicotinamide adenine dinucleotide phosphate or its 1,4-dihydro reduced form ($NADP^+$/NADPH) [9], and other small molecules (Fig. 1A). Additionally, macromolecular proteins (*e.g.*, thioredoxin [10] and its associated proteins [7]) play a role in this network (Fig. 1A). The entire network is interconnected and dynamically regulated in real time in response to external stimuli [2], making it challenging to use a single molecule to reflect the global redox status. In particular, *in situ* detection and evaluation of the intracellular thiols redox state relating to a wide range of reducing sulfur species (RSS) remains a significant challenge.

To monitor the thiols redox status, analytical methods such as thiol-based redox proteomic methods [11], indirect detection of metabolite marker by chromatography [12], genetically encoded tool [13], have been developed [14], but their inherent limitations make it difficult to perform real-time monitoring in living cells. Fluorescence sensing has become an important tool in the investigation of cellular biological functions based on its high temporal and spatial resolution and favorable biocompatibility. In the past decade, fluorescent probes have been developed for assessing the redox state of cells, mainly including the probes for detecting ROS [15,16], RSS-responsive probes [17-19], and genetically-encoded probes targeting low concentrations of $NADP^+$/NADPH [20], *etc.* Among them, the concentration of RSS, represented by GSH, has been an important marker for assessing the redox state

* Corresponding author.
E-mail address: x.l.sun86@xjtu.edu.cn (X. Sun).

https://doi.org/10.1016/j.cclet.2024.110528
1001-8417/

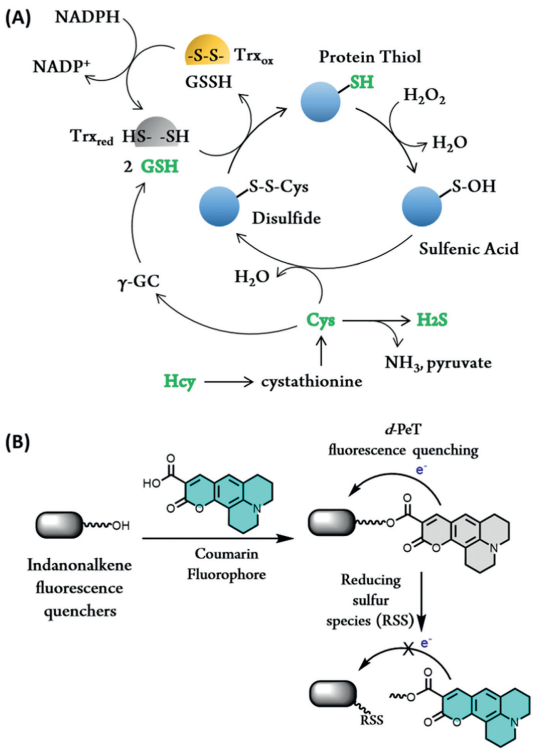

Fig. 1. (A) The network of cellular thiol redox system in multicellular eukaryotes. Cys is derived from extracellular cystine, which is a precursor of GSH, H_2S. Methionine is converted *via* the transsulfuration pathway first to Hcy and eventually to Cys. Cys residues located on the surface of redox-sensitive proteins can easily undergo ionization, and are then oxidized by H_2O_2 to sulfenic derivatives (-SOH). The NADPH-dependent thioredoxin system (Trx_{ox}/Trx_{red}) provides reducing equivalents for peroxiredoxins and is closely interconnected with GSH/glutaredoxins system. (B) Schematic illustration of the design of a fluorescence switching platform for the recognition of RSS. The molecule was initially non-fluorescent due to *d*-PeT, with coumarin acting as electron donor and a conjugated acceptor serving as electron acceptor. Upon cleavage in the presence of RSS species, the fluorescence is switched on.

of cells due to its high concentration and free permeation through the organelles [21-24]. However, most fluorescent probes specifically response to one or a few thiol molecules. Given that biothiols can rapidly interconvert under enzyme catalysis (Fig. 1A) [25], it is still challenging to reflect the global thiols redox state by targeting only a single molecule. Additionally, beyond small-molecule thiols, the conversion between sulfhydryl-disulfide bonds in Cys residues of proteins is a crucial intracellular oxidation–reduction regulator. Unfortunately, most current fluorescent probes overlook the impact of protein thiols, complicating the comprehensive assessment of the redox state.

Our group recently reported an indanonalkene photoluminescent platform based on a unified and modified conjugate acceptor (CA, Fig. S1 in Supporting information) [26,27]. We found that the conjugate acceptors from the platform could function as fluorescence quencher after linking with a fluorophore, thus revealing a new fluorescence quenching method for the design of small molecule-based fluorescent probe with donor-excited photo-induced electron transfer (*d*-PeT) mechanism (Fig. 1B). The reaction-based activable probe constructed in this work contains open-chain bis-vinylogous thioesters that are highly reactive towards RSS through thiol coupling and/or cyclization reactions, enabling real-time optical signal amplification *via* activity-based sensing. The probe not only recognizes small molecule biothiols, such as Cys, homocysteine (Hcy), GSH, and reactive sulfur species like H_2S, but also produces a significant fluorescence turn-on towards cysteine thiols on a protein while remaining insensitive

Table 1
Summary of photophysical properties of IC-1/2/3/4/5 and C-343.

Name	λ_{abs}[a]	λ_{em}[a]	ε[b]	Φ_f (%)[c]	τ (ns)[d]	ΔE (eV)[e]
C-343	443	461	1.1886	63	4.57	–
IC-1	438	483	2.8259	4.9	3.26	2.58
IC-2	456	492	1.0659	3.3	3.48	3.65
IC-3	447	488	1.2119	3.9	2.40	3.62
IC-4	440	484	1.9913	1.3	2.34	3.64
IC-5	440	484	3.2920	0.9	2.69	3.65

[a] Optimum absorbance (λ_{abs}) and fluorescence wavelength (λ_{em}) of chromophores.
[b] Molar extinction coefficient (ε) × 10^4 L mol^{-1} cm^{-1}.
[c] Relative quantum yields (QY, Φ_f).
[d] Average fluorescence lifetimes (τ) were calculated and fitted using multi-exponential equation.
[e] Calculated energy gap (ΔE) using the Gaussian program at the B3LYP/6–31+G(d) level of theory.

to their oxidized forms under ambient conditions, thus enabling global evaluation. Based on this, we investigated the performance of the probe in response to RSS in normal and oxidatively stimulated living cells, demonstrating rapidity, sensitivity, and high biocompatibility, which is expected to play an important role in real-time assessment of global redox status.

It was revealed previously that the molecule CA containing open-chain bis-vinylogous thioesters, would undertake addition-elimination and cyclization reactions towards thiol and amine derivatives [27,28]. Based on these findings, the fundamental conjugate acceptor was functionalized through thiol and amine coupling to generate CA-1/2/3/4 (Fig. S1). The derived acceptors with terminal hydroxyl group were then linked with coumarin (C-343) as a fluorophore through esterification to generate IC-1/2/3/4 (Fig. 2A and Fig. S1). Compound IC-4 was further modified through an amine-thiol scrambling to generate molecule IC-5 (Fig. S1). All the compounds were characterized using nuclear magnetic resonance (NMR) and high-resolution mass spectroscopy (HRMS) (see Supporting information).

Initially to understand the quenching effect of the system, we evaluated the photophysical properties for the molecules using experimental and computational analyses. From the ultraviolet–visible (UV–vis) spectra, two prominent peaks for each of the molecule were observed, respectively (Fig. 2B). The molar extinction coefficients (ε) for each of the molecule was calculated as $>10^4$ L mol^{-1} cm^{-1} (Table 1) based on the absorbent intensities. In the fluorescence spectra, the strong fluorescence intensity from coumarin ($\Phi_f = 63\%$) was significantly decreased after attachment to CA-1, confirming the quenching effect of the acceptor on IC-1 ($\Phi_f = 4.9\%$) (Fig. 2C and Table 1). Next, attachment of the *S,S*-cyclic moelcule CA-2 to coumarin also quenched the fluorescence to generate IC-2 ($\Phi_f = 3.3\%$). What is more, the amine coupled conjugate acceptors CA-4 and CA-5 led to enhanced quenching degree on coumarin C-343 (Table 1), resulting in quantum yield for IC-4: 1.3% and IC-5: 0.9%, respectively. Furthermore, by changing the length of the linker between the fluorophore and quencher, *i.e.*, IC-3 and IC-4, the relative quantum yields decreased from 3.9% of IC-3 to 1.3% of IC-4. Additionlly, the shortened fluorescence lifetime (Table 1 and Fig. S2 in Supporting information) of probes IC-1 to 5 (2.34–3.48 ns) compared to C-343 (4.57 ns) also validates the efficient excited state quenching.

Next, density functional theory (DFT) calculations were carried out to understand the fluorescence quenching behaviors (Fig. 2D and Fig. S3 in Supporting information). From the DFT remodeling, the electrons were mostly distributed on the planar section of coumarin on highest occupied molecular orbital (HOMO) before excitation for all the molecules. Upon excitation, intramolecular electron transfer from the excited state of the fluorophore to

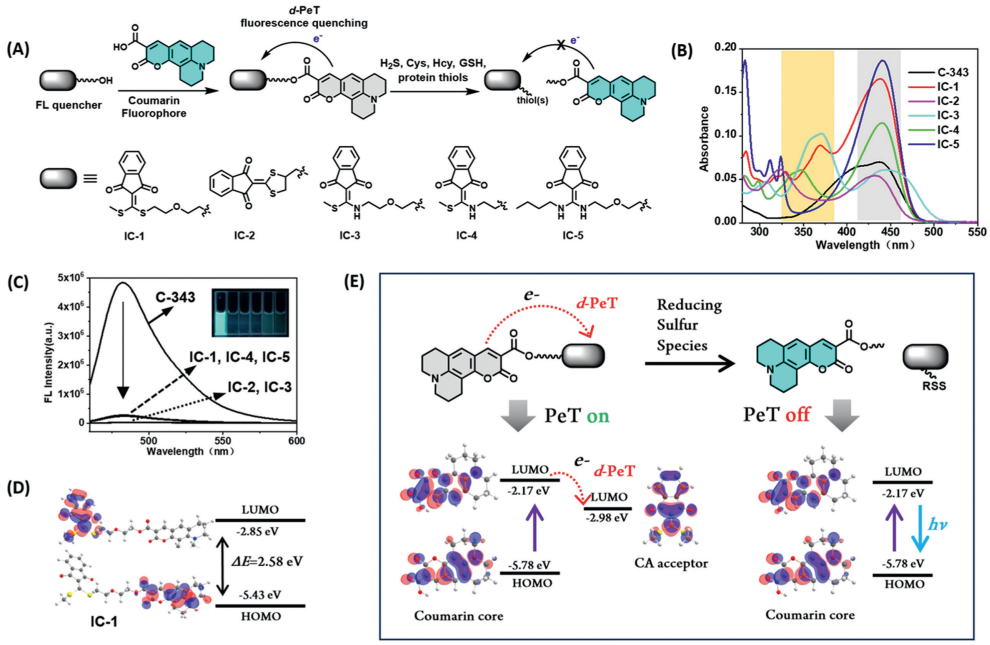

Fig. 2. (A) Schematic illustration of the design and synthesis of molecular probes IC-1 to IC-5. (B) UV–vis absorbance spectra and (C) fluorescence spectra of IC-1 to IC-5 and C-343 in DMSO (5 μmol/L, λ_{ex} = 450 nm). Insets: from left to right, are photographs of C-343 and IC-1 to −5 under 365 nm excitation. (D) Schematic frontier molecular orbital energy diagrams of the IC-1, respectively. All the geometries of compounds were optimized at B3LYP/6–31+G(d) level. (E) Schematic frontier molecular orbital energy diagrams of the *d*-PeT process of IC-1 before and after reaction with RSS.

the conjugate acceptors on lowest unoccupied molecular orbital (LUMO) occurred, as a result of attenuated fluorescence emission. The values calculated for the energy gaps for each of the molecular probes were between 2.5 eV and 3.7 eV, which matched the UV–vis absorbance (Fig. 2 and Table 1).

Additionally, the feasibility of the PeT process within IC-1 to IC-5 can be predicted by comparing the LUMO energy level of the electron donor (the coumarin unit) and the electron acceptor (the CA moiety). As shown in Fig. 2E, the LUMO level of the CA (−2.98 eV) is lower than that of the coumarin unit (−2.17 eV) which facilitates the electron transfer, thus intramolecular PeT would occur, and IC-1 was weakly emissive. Once the covalent bonding between the CA and coumarin was cut off, the LUMO energy level from CA was then elevated higher than the LUMO of fluorophore, thus recovering the fluorescence emission (see right). So far, it was confirmed that the acceptor-mediated quenching proceeds *via* a *d*-PeT from electron rich C-343 to electron poor acceptor, and this rule can be generalized in the cases of different conjugate acceptors, *i.e.*, CA-1/2/3/4/5.

Among the fluorescence probes given above, molecular IC-1 comprises of open chain bis-vinylogous thioesters which are good leaving groups, that undergo “click“ reactions with nucleophiles under biological conditions (Fig. 3A). While the other molecules, *i.e.*, IC-2 to IC-5 with either *S*,*S*-cyclic or amine-coupled acceptors exhibit reduced reactivity probably due to their thermostability. To verify the assumption, all the molecules were reacted with 100 μmol/L of H_2S, Cys, Hcy, and GSH, respectively under neutral phosphate buffered saline (PBS) at room temperature for 1 h, after which fluorescence changes were measured (Fig. 3B and Fig. S4 in Supporting information). It can be observed that only IC-1 exhibited a significant fluorescence “turn-on” in the presence of the thiol species. In this regard, fluorescent probe IC-1 was selected as the candidate for the detection of RSS species in the following experiments.

Among the RSS, H_2S is the predominant form of reactive sulfur species, which is also an important gasotransmitter in signaling pathways [29]. Reduced thiols in biological organisms, *e.g.*, Cys, Hcy and GSH, all contain reactive thiol groups as part of their chemical structure and are important biomarkers in live cells [30]. Next, the reaction kinetics of IC-1 with the biothiols was tracked by monitoring the UV–vis absorption and fluorescence emission under neutral PBS buffer conditions. For the UV–vis spectra (Fig. S5 in Supporting information), the absorption peak at λ_{abs2} = 450 nm was almost stable while the absorption peak around λ_{abs1} = 410 nm decreased and new peaks at shorter wavelengths (295–377 nm) gradually formed in the presence of H_2S, Cys, Hcy, GSH respectively. The changes of absorbance indicted that chemical reactions occurred between all the RSS species and the probe. In terms of emission, time-dependent fluorescence intensity increases of IC-1 can be seen upon addition of different thiols respectively (Fig. 3C and Fig. S6 in Supporting information), it can be observed that the fluorescence signal at λ_{em} = 490 nm from reaction between IC-1 and GSH reached maximum within 20 min while H_2S, Cys and Hcy took a longer time but ended with stronger fluorescence responses within 120 min. And Hcy showed a more rapid reaction probably due to the formation of a thermodynamically stable six-membered ring (CA-Hcy). The results as described above confirm that IC-1 exhibits turn on fluorescence response after interaction with small molecular biothiols under ambient conditions.

To further investigate the reaction mechanism of the small molecular biothiols with IC-1, the products after reaction were characterized using high-resolution mass spectroscopy (HRMS) *in situ* (Fig. S7 in Supporting information). As can be seen from Fig. S7A, the peak at *m/z* = 390.137 (calcd. for $C_{20}H_{23}NO_5S$ $[M+H]^+$ 390.137) corresponds to HS-C343 was determined for each of the reactions of IC-1 with the four sulfur species, suggesting that the release of the thiol-terminated coumarin from the probe after reaction.

Next, the other product CA-H_2S released from reaction between H_2S and IC-1 was confirmed through a negative mode HRMS (Fig. S7B, *m/z* = 234.989 for $C_{11}H_8O_2S_2$ $[M-H]^-$). In addition, the products CA-Cys (Fig. S7C, *m/z* = 276.033 for $C_{20}H_{23}NO_5S$ $[M+H]^+$) and CA-Hcy (Fig. S7D, *m/z* = 290.048 for $C_{20}H_{23}NO_5S$ $[M+H]^+$) were identified as the main species from the HRMS spectra due to the

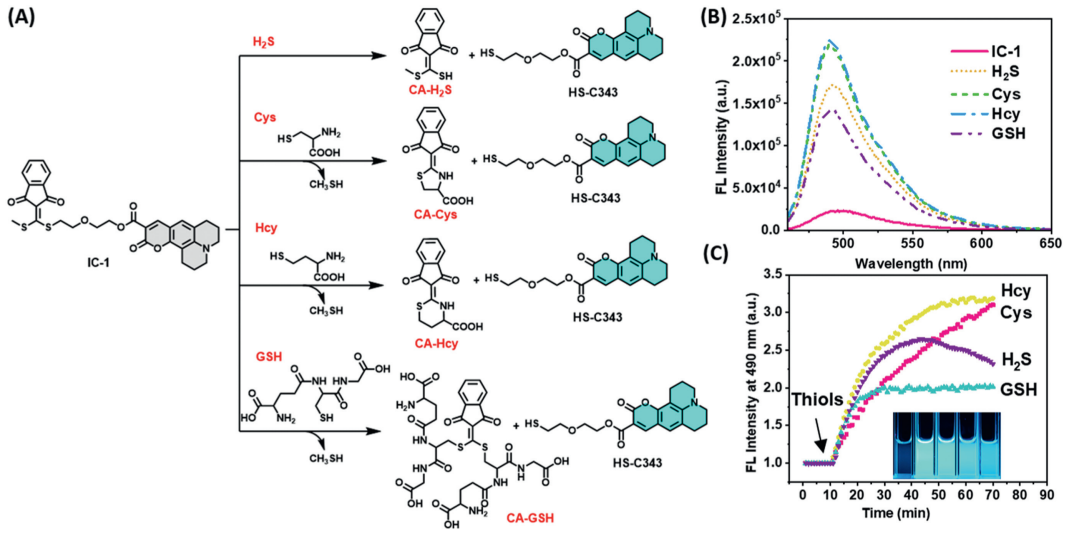

Fig. 3. Chemical reaction and optical responses of IC-1 towards RSS. (A) Chemical reactions between IC-1 and H_2S, Cys, Hcy, GSH under neutral aqueous condition to generate the cyclic products CA-H_2S, CA-Cys, CA-Hcy through thiol-amine coupling and CA-GSH through thiol-thiol exchange(s). The released fluorophore HS-C343 recovers its fluorescence through reduced *d*-PeT quenching. (B) Initial fluorescence spectra of IC-1 (1 μmol/L) and fluorescence spectra after 60 min of reaction with H_2S, Cys, Hcy, GSH (100 μmol/L), respectively. Excited by 450 nm. Slit: 2 nm/2 nm. (C) Kinetics for IC-1 (1 μmol/L) in the presence of H_2S, Cys, Hcy, GSH (100 μmol/L), respectively over 60 min in pH 7.4 PBS (1% DMSO as co-solvent). Insets: from left to right, are photographs of IC-1 after 60 min reaction with Hcy, Cys, H_2S, GSH under 365 nm excitation.

cyclization reaction inuduced by Cys/Hcy, respectively. Further, the reaction between IC-1 and GSH generated both mono-substituted CA-GSH (Fig. S7E, $m/z = 510.100$ for $C_{21}H_{23}N_3O_8S_2$ $[M+H]^+$) and bis-substituted CA-2GSH (Fig. S7F, $m/z = 769.180$ for $C_{30}H_{36}N_6O_{14}S_2$ $[M+H]^+$) products after thiol-thiol scrambling with IC-1. Further to confirm the function of the thiols on the reactions, oxidized Cys (*i.e.*, cystine) and glutathione oxidized (GSSG) with disulfide bonds were prepared and almost non-fluorescent responses occurred in the raction with IC-1 (Fig. S8 in Supporting information). These confirm the specificity of the probes for the detection of RSS *in situ*, which is critical for biological applications (see below). Furthermore, we tested the fluorescence turn on of the probe at different pH (Fig. S9 in Supporting information) using Cys as an example, and showed that alkaline environment promotes the speed of thiol recognition. In a short summary, typical RSS all exhibited high reactivity towards the probe due to addition-elimination reactions on the reactive sites of the bis-vinylogous thioesters on the conjugate acceptor.

Interconversion between sulfhydryl and disulfide bonds playing vital roles during cellular homeostasis and cell signaling, which is critical for the maintenance of cellular redox balance [31]. The majority of Cys residues on proteins are in the form of disulfide bonds, so the abundance of reduced thiols on protein is lower than the small molecule RSS, even some of them are located in specific structural domains that are difficult to be detected [32]. Therefore, we further investigated the performance of IC-1 for the detection of reduced sulfhydryl groups on proteins [27,33].

Bovine serum albumin (BSA) was chosen as the model protein and was reduced by tris(2-carboxyethyl)phosphine (TCEP) to break its disulfide bonds and expose free sulfhydryl groups to obtain reduced BSA (rBSA) (Fig. 4A). IC-1 was then reacted with BSA and rBSA, respectively, and the UV absorption spectra and fluorescence spectra were monitored for time-dependent changes (Fig. S10 in Supporting information), which exhibited 15.6-fold fluorescence enhancement and an absorption enhancement at $\lambda = 450$ nm in the presence of rBSA, in contrast to BSA exhibited almost no changes. Consistent properties and similar trends were also observed when using another model protein, reduced lysozyme (Fig. S11 in Supporting information), confirming the universality for detecting thiols on reduced proteins. In a dose dependent titration (Fig. 4B), the fluorescence intensity at 490 nm exhibited a strong linear correlation ($R^2 = 0.9937$) with rBSA concentrations (0.01–0.09 μmol/L) in Fig. 4C, and the limit of detection (LOD = $3\sigma/k$) was calculated to be 0.8 nmol/L, which enables detection of low abundant protein thiols in biological systems. In addition, by adjusting the amount of reducing reagent TCEP, BSA with different amounts of free thiols was obtained, and the fluorescence turn-on after reacting with an equal dose of probe is shown in Fig. 4D. The linear dependence on TCEP concentrations of 0–5 equiv. confirms that protein thiol content can be quantitatively detected by the IC-1 over a certain range (Fig. 4E). In addition, the fluorescence intensity of the probe indicates the degree of reduced protein, independent of the protein content.

In the selectivity test, we then compared the fluorescence turn-on responses of IC-1 induced by rBSA with other fifteen amino acids, small molecule amines, and TCEP (Fig. 4F). It can be observed that IC-1 is most sensitive towards low concentrations of rBSA (10 μmol/L), followed by H_2S, Cys, Hcy, and GSH, whereas it barely reacts with other thiol-free amino acids (Trp, Leu, Phe, Glu, Tyr, Asp, Lys, Thr, Ser, Pro, Ala, Gly, Met), amines (ethylenediamine, butylamine), and TCEP reductants (Fig. 4F). All these indicate that IC-1 could be used to detect biothiols in complex biological environments, independent of other amino acids, reducing agents, *etc.* A further comparison of the reaction kinetics of IC-1 towards different biothiols is given in Fig. 4G. The reaction with rBSA (10 μmol/L) reached equilibrium within only 5 min, more rapid than the other biothiols even with concentrations of 100 μmol/L. It is reasoned that the particular hydrophobic microenvironment or confinement effect on the protein structural domain as well as the fact that the two thiols with stronger nucleophilicity are proximal, enhances the molecular interactions and thus results in the rapid reaction (Fig. 4A).

Encouraged by the above results, we investigated probe IC-1 for the detection and imaging of RSS in living cells. The cytotoxicity of IC-1 was firstly assessed using an MTT assay (Fig. S12 in Supporting information), and it displayed good biocompatibility during co-incubation with both human hepatoma HepG2 and EMT-6 cell line over 24 h. Next, the imaging of intracellular endogenous RSS by IC-1 was then investigated. The results of dose-dependent (Fig. S13 in Supporting information) fluorescence imaging revealed that cellu-

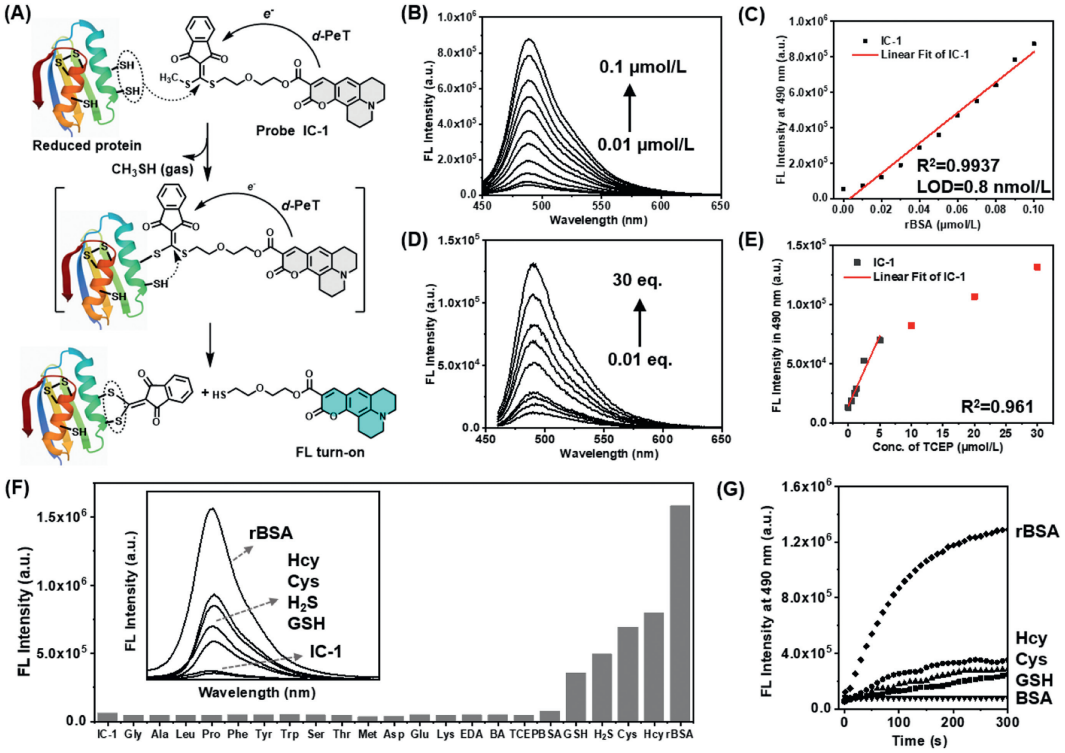

Fig. 4. (A) Chemical reactions and fluorescence response towards reduced cysteine residues in proteins. (B) Fluorescence spectra of the probe IC-1 (1 μmol/L) after reaction with different concentrations (0.01–0.09 μmol/L) of rBSA in pH 7.4 PBS (1% DMSO as co-solvent) at room temperature for 1 h. Excited at 400 nm. Slit (nm): 2/2. (C) The linear changes of the fluorescence intensity at 490 nm of IC-1 as a function of rBSA concentration. (D) Fluorescence spectra of the probe IC-1 (1 μmol/L) after 1 h of reaction with BSA (10 μmol/L) reduced by different equivalents (0.01, 0.5,1, 1.25, 2.5, 5, 10, 20, 30) of TCEP. (E) The relationship between fluorescence intensity at 490 nm and TCEP equivalents in (D). (F) Comparison of fluorescence intensity at 490 nm after 1 h of reaction of 1 μmol/L IC-1 with 10 μmol/L BSA and rBSA, 100 μmol/L H_2S, Cys, Hcy, GSH and other 13 natural amino acids (Gly, Ala, Leu, Pro, Phe, Tyr, Trp, Ser, Thr, Met, Asp, Glu, Lys), 100 μmol/L small molecule amines (EDA: Ethylenediamine; BA: Butylamine) and reductant TCEP, respectively. Inset spectra indicate the fluorescence emission of IC-1 upon adding various species. (G) Comparison of reaction kinetics of different biothiols with IC-1 (1 μmol/L). rBSA/BSA concentration is 10 μmol/L while the others are 100 μmol/L.

lar fluorescence could be observed even at low concentrations with 2.5 μmol/L of IC-1, demonstrating that IC-1 penetrates cells efficiently and can be used for intracellular detection. Time-dependent imaging (Fig. S14 in Supporting information) indicated that 30 min of incubation resulted in the atinment of equilibrium, so this condition was chosen for subsequent experiments. In addition, the images obtained reflect the distribution of RSS in certain organelles, as shown by multichannel co-localization imaging (Fig. 5A and Fig. S15 in Supporting information) with commercially available organelle dyes mitochondria tracker, lysosome tracker, and endoplasmic reticulum (ER) tracker, respectively, the probe exhibits a higher Pearson correlation coefficient ($r = 0.92$) with the ER. The intensity distribution of the two channels at the line of interest (Fig. S15) also illustrates a high coincidence with the ER. Previous studies have suggested that ER proteins have higher oxidation levels compared to other organelles [34], but our results show that the ER luminal still has a high amount of free RSS, possibly originating as a byproduct of enzyme-catalyzed redox reactions.

To further validate the specific responses of IC-1 towards biothiols in living cells, we adjusted the intracellular biothiol content with *N*-ethylmaleimide (NEM) and dithiothreitol (DTT) to block and increase the intracellular thiol levels, respectively (Fig. 5B). In the experiment, IC-1 was added after removal of the treatment agent, and the fluorescence intensity of the cells was measured after 30 min (Figs. 5B and C). It can be seen that compared to the untreated group (Figs. 5Bi and 5Ci), the fluorescence intensity of 0.5 mmol/L NEM-treated cells were slightly reduced (Figs. 5Bii and 6Cii), while the fluorescence was enhanced by 0.5 mmol/L DTT treatment (Figs. 5Biii and 5Ciii). Additionally, cells of group ii were then treated with exogenous 1 mmol/L Cys, Hcy, and GSH (Figs. 5Biv, v, vi), and the fluorescence intensity was greatly enhanced (Figs. 5Civ, v, vi), higher than group i and ii, confirming the biothiol-specific response of IC-1. Here, we observed fluorescence in the nucleus after NEM treatment, presumably due to an increase in the permeability of the nucleus induced by reductive NEM and probe penetration into the nucleus. The intracellular content of RSS is closely related to the cellular redox state, and the accumulation of ROS in oxidative stress is accompanied by the depletion of large quantities of reduced species to resist oxidative damage [2,5]. We further investigated the response of IC-1 to cellular oxidative stress. The mitochondrial respiratory chain was blocked by treating with different concentrations (0.5–2 μmol/L) of rotenone to induce cellular oxidative stress, while the commercial ROS probe dihydroethidium (DHE) was used to indicate the ROS content, and the results are shown in Figs. S16 and S17 (Supporting information). It can be seen that cells under normal incubation conditioning (Figs. S16A–C) were abundant in RSS with no obvious accumulation of ROS; after 1 h of pre-incubation with rotenone (Figs. S16D–F), the ROS content was elevated with the increasing concentration of rotenone, while the IC-1 fluorescence channel showed a general decrease compared to the control group, with the 1 μmol/L-treated group (Figs. S16E and S17) being the most significant. It was observed that the distribution of green fluorescence in the cells also became more diffuse. The above results showed that intracellular reduced thiols were depleted as ROS accumulated, but the global thiols oxidation level did not strictly correlate with ROS content.

Ferroptosis is a regulated form of cell death that is distinct from apoptosis, autophagy, *etc.* and has attracted increasing attention owing to numerous organ injuries and degenerative pathologies that are caused by ferroptosis [35]. It has been suggested that

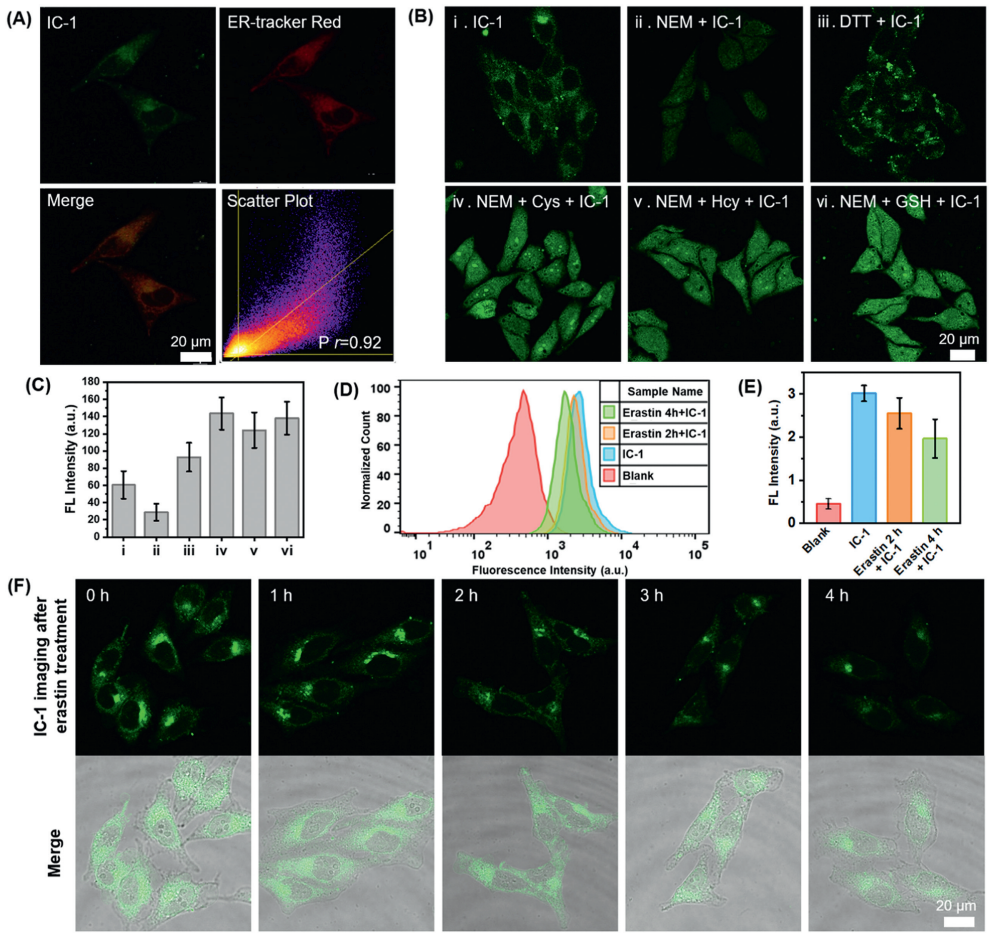

Fig. 5. (A) Merged confocal fluorescence image of HepG2 cells after co-staining with IC-1 (green channel) and ER-tracker (red channel) and the corresponding intensity scatter plot. (B) Fluorescence imaging of biothiols using IC-1 in HepG2 cells under different treatments. (i) 5 μmol/L IC-1, 30 min; (ii) 500 μmol/L NEM for 30 min, then 5 μmol/L IC-1 for 30 min; (iii) 500 μmol/L DTT for 30 min, then 5 μmol/L IC-1 for 30 min; 500 μmol/L NEM for 30 min, then 1 mmol/L Cys (ix)/Hcy (x)/GSH (xi) for 30 min, 5 μmol/L IC-1 for 30 min at last (λ_{ex} = 450 nm, λ_{em} = 500–550 nm). (C) Relative fluorescence intensity of the corresponding image of (B). (D) Flow cytometric analysis of endogenous biothiols by IC-1 between 1 h and 4 h pre-incubation with ferroptosis inducer (erastin, 10 μmol/L) in HepG2 cells. Detection channel: 405 nm laser light source with a 525/50 band-pass filter. (E) Quantification of mean fluorescence intensity per cell (20,000 cells in total), referring to different groups in (D). Significant differences were analyzed using unpaired *t*-test program through the statistical software GraphPad Prism 9.0. (F) Time-dependent (1–4 h) confocal fluorescence images of endogenous RSS by IC-1 in erastin treated HepG2 cells (λ_{ex} = 450 nm, λ_{em} = 500–550 nm). The values are mean ± *s*.d. (n = 5).

cellular ferroptotic death is driven by lipid peroxidation [36], as mentioned earlier, intracellular biothiols are directly related to the redox status, therefore, oxidative stress is highly possible during ferroptosis, resulting in fluctuations of global thiols redox level. Therefore, we next evaluated RSS changes during ferroptotic death using the thiol-responsive small molecular probe IC-1. As shown in Figs. 5D–F, HepG2 cells were co-incubated with the ferroptosis-inducer erastin (a cystine transporter inhibitor) for one to four hours to obtain cells at different stages of programmed cell death. After removal of the inducer, IC-1 was added and incubated for an additional 30 min to ensure full reaction with the biothiols, and then tracked by flow cytometric analysis (Figs. 5D–F), respectively. The results indicate that compared to normal cells, the fluorescence intensity of the cells decreased, as the induction time was prolonged, with the average fluorescence intensity dropping by approximately 70% of the untreated group after 4 h of treatment, and flow cytometric analysis confirmed these results. Thus, by inhibiting the activity of amino acid transporter system x_c^-, erastin leads to the depletion of reducing substances such as Cys and GSH with prolonged incubation time, and the continuous decrease of the total RSS, inducing the peroxidation of phospholipids, and further facilitating the process of ferroptosis.

In summary, we developed a fluorescence switching molecular platform through incorporating a series electron-deficient conjugate acceptors with a single electron-rich fluorophore. The mode of action of the platform was confirmed by DFT as *d*-PeT, as a mechanism to explain the photoluminescent quenching effect. The activity-based small molecular probe was investigated based on the response towards RSS and biothiols, *i.e.*, H_2S, Cys, GSH, Hcy. Probe IC-1 with proximal dual reactivity exhibited a rapid and low limit of detection towards vicinal dithiol-containing proteins (rBSA as a model, LOD = 8 nmol/L). Furthermore, the probe exhibited low toxicity and good cell permeability and was used to assess the content of endogenous RSS under different oxidative/reducing treatment conditions, and achieved the detection of global thiols redox level during ferroptosis, confirming the potential of the probe for the detection of multiple types of biothiols. In summary, we developed a multi-responsive fluorescent probe towards reduced sulfur species for a comprehensive evaluation of the global intracellular content of almost all possible forms of reduced sulfur species. We hope that our fluorescence switching molecular platform will inspire more groups to explore the design of functional molecules for biomarker sensing, such as near-infrared probes for deep tissues, and the development of probes suitable for biomedical research.

Declaration of competing interest

The authors declare that they have no known competing financial interests or personal relationships that could have appeared to influence the work reported in this paper.

CRediT authorship contribution statement

Hui Zhang: Writing – original draft, Methodology, Funding acquisition, Data curation, Conceptualization. **Rong Feng:** Methodology, Formal analysis, Data curation. **Wanyi Yu:** Methodology, Formal analysis, Data curation. **Hongbei Wei:** Methodology, Investigation, Data curation. **Tianhong Wu:** Methodology, Investigation, Data curation. **Peng Zhang:** Methodology, Investigation, Data curation. **Wenhai Bian:** Investigation, Formal analysis, Data curation. **Xin Li:** Writing – review & editing, Visualization, Software. **Di Gao:** Writing – review & editing, Validation, Conceptualization. **Guojun Weng:** Writing – review & editing, Validation, Conceptualization. **Zhe Yang:** Writing – review & editing, Supervision, Conceptualization. **Xiaolong Sun:** Writing – review & editing, Supervision, Project administration, Funding acquisition, Conceptualization.

Acknowledgments

The authors thank the National Natural Science Foundation of China (Nos. 21907080, 22278330) and Youth Innovative Team (No. xtr052022012), Fundamental Research Funds for the Central University (No. xzy012023010) from Xi'an Jiaotong University. This work was also supported by Natural Science Basic Research Program of Shaanxi (No. 2023-JC-QN-0246), China/Shaanxi Postdoctoral Science Foundation (Nos. 2023M732811, 2023BSHEDZZ20). TDJ wishes to thank the University of Bath and the Open Research Fund of the School of Chemistry and Chemical Engineering, Henan Normal University (No. 2020ZD01) for support. We also thank Professor Xuhong Qian (East China Normal University) for the discussion and suggestions.

Supplementary materials

Supplementary material associated with this article can be found, in the online version, at doi:10.1016/j.cclet.2024.110528.

References

[1] G.J. McBean, M. Aslan, H.R. Griffiths, R.C. Torrão, Redox Biol. 5 (2015) 186–194.
[2] H. Sies, R.J. Mailloux, U. Jakob, Nat. Rev. Mol. Cell Biol. 25 (2024) 701–719.
[3] D.A. Butterfield, M. Perluigi, Antioxid. Redox Signal. 26 (2016) 277–279.
[4] E.C. Cheung, K.H. Vousden, Nat. Rev. Cancer 22 (2022) 280–297.
[5] H. Sies, V.V. Belousov, N.S. Chandel, et al., Nat. Rev. Mol. Cell Biol. 23 (2022) 499–515.
[6] G.D. Ferguson, W.J. Bridge, Redox Biol. 24 (2019) 101171.
[7] G. Filomeni, E. Desideri, S. Cardaci, G. Rotilio, M.R. Ciriolo, Autophagy 6 (2010) 999–1005.
[8] K. Ulrich, U. Jakob, Free Radical Biol. Med. 140 (2019) 14–27.
[9] R.J. Mailloux, J.R. Treberg, Redox Biol. 8 (2016) 110–118.
[10] R. Gencheva, E.S.J. Arnér, Annu. Rev. Pharmacol. Toxicol. 62 (2022) 177–196.
[11] Z. Su, J.G. Burchfield, P. Yang, et al., Nat. Commun. 10 (2019) 5486.
[12] H. Liu, F. Xu, Y. Gao, et al., Anal. Chem. 92 (2020) 8810–8818.
[13] V. Cracan, D.V. Titov, H. Shen, Z. Grabarek, V.K. Mootha, Nat. Chem. Biol. 13 (2017) 1088–1109.
[14] L.R. Knoke, L.I. Leichert, Curr. Opin. Chem. Biol. 77 (2023) 102390.
[15] X. Chen, F. Wang, J.Y. Hyun, et al., Chem. Soc. Rev. 45 (2016) 2976–3016.
[16] H. Ren, Y. Du, X. Yang, et al., Chin. Chem. Lett. 36 (2025) 109867.
[17] C.X. Yin, K.M. Xiong, F.J. Huo, J.C. Salamanca, R.M. Strongin, Angew. Chem. Int. Ed. 56 (2017) 13188–13198.
[18] Y. Yang, M. Ma, L. Shen, et al., Angew. Chem. Int. Ed. 62 (2023) e202310408.
[19] T. Jin, M. Cui, D. Wu, et al., Chin. Chem. Lett. 32 (2021) 3899–3902.
[20] Y. Zhao, Q. Hu, F. Cheng, et al., Cell Metab. 21 (2015) 777–789.
[21] N. Patsoukis, C.D. Georgiou, Anal. Bioanal. Chem. 383 (2005) 923–929.
[22] K. Umezawa, M. Yoshida, M. Kamiya, T. Yamasoba, Y. Urano, Nat. Chem. 9 (2017) 279–286.
[23] H. Chen, Y. Tang, W. Lin, TrAC Trends Anal. Chem. 76 (2016) 166–181.
[24] W. Liu, C.N. Yang, Z.L. Yang, et al., Angew. Chem. Int. Ed. 62 (2023) e202304023.
[25] A. Domán, É. Dóka, D. Garai, et al., Redox Biol. 60 (2023) 102617.
[26] X. Feng, T. Wu, X. Sun, X. Qian, J. Am. Chem. Soc. 143 (2021) 21622–21629.
[27] P. Zhang, X. Wang, X. Wang, et al., Anal. Chem. 95 (2023) 11953–11959.
[28] T. Wu, W. Bian, C. Wang, et al., Aggregate 4 (2023) e295.
[29] K.G. Fosnacht, M.D. Pluth, Chem. Rev. 124 (2024) 4124–4257.
[30] L. Zhang, L. Zhang, X. Zhang, et al., TrAC Trends Anal. Chem. 169 (2023) 117377.
[31] M. Griffith, A. Araújo, Redox Biol. 69 (2024) 103000.
[32] J. van der Reest, S. Lilla, L. Zheng, S. Zanivan, E. Gottlieb, Nat. Commun. 9 (2018) 1581.
[33] C. Huang, T. Jia, M. Tang, et al., J. Am. Chem. Soc. 136 (2014) 14237–14244.
[34] J. Duan, T. Zhang, M.J. Gaffrey, et al., Redox Biol. 36 (2020) 101649.
[35] X. Jiang, B.R. Stockwell, M. Conrad, Nat. Rev. Mol. Cell Biol. 22 (2021) 266–282.
[36] M. Conrad, D.A. Pratt, Nat. Chem. Biol. 15 (2019) 1137–1147.